

A Cox rate-and-state model for monitoring seismic hazard in the Groningen gas field

Z. Baki ^a and M.N.M. van Lieshout ^{b,a}

^a Faculty of Electrical Engineering, Mathematics and Computer Science, University of Twente, P.O. Box 217, NL-7500 AE, Enschede, The Netherlands.

^b CWI, P.O. Box 94079, NL-1090 GB Amsterdam, The Netherlands

Abstract: To monitor the seismic hazard in the Groningen gas field, we modify the rate-and-state model that relates changes in pore pressure to induced seismic hazard by allowing for noise in pore pressure measurements and by explicitly taking into account gas production volumes. We analyse the first and second-moment structure of the resulting Cox process, propose an unbiased estimating equation approach for the unknown model parameters and derive the posterior distribution of the driving random measure. We use a parallel Metropolis adjusted Langevin algorithm for sampling from the posterior and to monitor the hazard.

Keywords: Cox process, gas production, induced seismicity, pore pressure, rate-and-state model, spatio-temporal point process.

Mathematics Subject Classification (MSC 2020): 60G55, 62F15, 62M30.

1 Introduction

The study of induced earthquakes caused by extraction or injection of fluids or gases is an important research topic. In the Netherlands, the Groningen gas field discovered in the late 1950s has played an important role in the Dutch economy. With an estimated recoverable gas volume of over 2,900 billion Normal cubic metres spread over a region of about 900 square kilometres, it is one of the largest gas fields on the planet [9]. However, large production volumes in the 1970s caused a drop in pore pressure in the gas field which resulted in induced earthquakes in the previously seismically inactive region. Thus, it is essential to be able to predict seismic hazard based on field measurements, for instance of pore pressure or, equivalently, Coulomb stress. One of the most widely used methodologies to do so is the rate-and-state model [3, 6, 14] which is now considered to be the state-of-the-art technique [10].

In the rate-and-state model (e.g. Candela et al. [3], Dempsey and Suckale [6] and Richter et al. [14]), the earthquakes follow a Poisson point process whose intensity function λ (the rate) is assumed to be inversely proportional to a state variable Γ that is defined by an ordinary differential equation. This differential equation is based on physical considerations and takes into account the elapsed time and the change in pore pressure. Nevertheless, it can

be criticised on several points. Firstly, since, by definition, the points in any Poisson point process do not interact with one another, the model is unable to deal with clustering as seen in, for instance, the Groningen data [11]. Secondly, the pressure values are assumed to be known everywhere. Lastly, the varying gas extraction is not taken into account. Our goal is to propose stochastic rate-and-state models that address these shortcomings and to develop a toolbox for statistical inference.

The plan is as follows. First, we briefly describe the data at our disposal and review the Poisson rate-and-state model. In Section 3, we propose a modified Cox rate-and-state model. We give explicit expressions of the first and second moments of the state variable in Section 4 and apply the delta method to approximate the first two moments of the rate variable. Some illustrations of the accuracy of the approximations for various pore pressure scenarios are given too (cf. Section 5). In Section 6, we turn to the estimation of the model parameters. Next, Section 7 focuses on the random state variable. We calculate its posterior distribution given earthquake count data and study a parallel Metropolis adjusted Langevin monitoring algorithm, which is next applied to the Groningen data. We close with a discussion and some suggestions for future research.

2 The Groningen gas field

2.1 Data

Figure 1 shows the spatial and temporal projections of the 332 earthquakes of magnitude 1.5 or larger that occurred from January 1st, 1995, up to December 31st, 2021, in the Groningen gas field¹. Note that earthquakes seem to happen more often in the central and southwestern parts of the gas field. Temporally, the steeper curve in the 1990s reflects the longer spell between successive earthquake occurrences; flatter pieces indicate a quicker succession of earthquakes.

To explain the observed heterogeneity, two covariates are at our disposal. Monthly production values from the start of preliminary exploration in February 1956 up to and including December 2021 were kindly provided to us². Additionally, 2009 pore pressure observations are available over the period from April 1960 until November 2018³. For a fuller discussion, we refer to [11].

2.2 The Poisson rate-and-state model

In the classic rate-and-state model [3, 6], earthquakes occur according to a spatio-temporal Poisson point process with intensity function

$$\lambda(s, t) = r_0 \frac{\Gamma(s, 0)}{\Gamma(s, t)}, \quad (s, t) \in W_S \times W_T, \quad (1)$$

¹Catalogue from www.knmi.nl, shapefiles from www.nlog.nl downloaded April 2022

²Mr Rob van Eijs from Shell

³nam-feitenencijfers.data-app.html/gasdruk.html

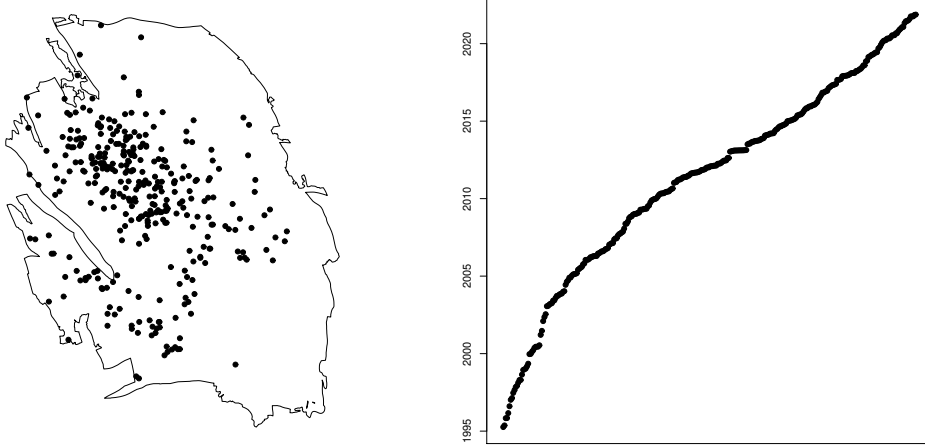


Figure 1: Spatial (left-most panel) and temporal (right-most panel) projections of the 332 earthquakes of magnitude 1.5 or larger with epicentre in the Groningen gas field that occurred in the period from January 1st, 1995, up to December 31st, 2021.

where $W_S \subset \mathbb{R}^2$ is a compact subset of the plane and W_T a closed and bounded interval in \mathbb{R} . The parameter $r_0 > 0$ is the background seismicity, the state variable $\Gamma(s, t)$ is defined by the ordinary differential equation

$$d\Gamma(s, t) = \alpha [dt + \Gamma(s, t)dX(s, t)],$$

where $X(s, t)$ is the pore pressure at spatial location s and time t and $\alpha > 0$. Multiplying both sides by $\exp(-\alpha X(s, t))$, discretising in time steps of length $\Delta > 0$ and writing $t_k = t_0 + k\Delta$ for the k -th point from $t_0 = \min\{t : t \in W_T\}$, $k = 1, \dots, m$, we obtain the Euler difference equation

$$\Gamma(s, t_{k+1}) = (\Gamma(s, t_k) + \alpha\Delta) \exp[\alpha(X(s, t_{k+1}) - X(s, t_k))], \quad s \in W_S. \quad (2)$$

The parameters r_0 , α and the initial state $\Gamma(s, t_0) \equiv \gamma_0 > 0$ are treated as unknowns and can be estimated, for example, by the maximum likelihood method. For a full discussion and comparison with other techniques, we refer to [10]. In line with current practice, we also discretise the spatial domain W_S in a regular grid with cell representatives s_1, \dots, s_n . Note that because W_S is not necessarily rectangular, grid cells may have different areas, which we shall denote by $\Delta(s_i)$.

3 The Cox rate-and-state model

The Poisson rate-and-state model of Section 2.2 expresses the change in seismic hazard in terms of elapsed time and pore pressure change. In practice, the values of the latter are typically available only at wells and monitoring stations. At other locations, the pore pressure must be estimated [11] or approximated by linear (or spline-based) interpolation [14]. For the Groningen data described in Section 2.1, there are only some two thousand observations scattered unevenly over the field and spanning a period of more than sixty years. Therefore, it would be better to explicitly take the uncertainty into account and model the $X(s_i, t_j)$ as a random variable. By doing so, we obtain a doubly stochastic or Cox point process [5]. Briefly, given a realisation λ of the density Λ of a random measure on $W_S \times W_T$, the driving random measure of the Cox process, the earthquakes form a Poisson process with intensity function λ . Thus, the distribution of the Cox process is fully characterised by the distribution of the driving random measure.

To find a suitable driving random measure, we assume that the pore pressure can be decomposed in a deterministic and stochastic part, that is,

$$X(s_i, t_j) = c(s_i, t_j)^\top \beta + E(s_i, t_j) \quad (3)$$

for some known function c with values in \mathbb{R}^p , unknown parameter $\beta \in \mathbb{R}^p$ and independent mean-zero random variables $E(s_i, t_j)$ with variance σ^2 . The parameters β and σ^2 can then be estimated by the least squares method. For our data, as in [11], without recourse to further explanatory variables, we let c be a polynomial of order four in space, of order two in time and add interaction terms up to first order in time and third order in space. For brevity, we will write $m(s_i, t_j) = c(s_i, t_j)^\top \hat{\beta}$ from now on. The variogram of the residuals is flat in time. The residual spatial variation $U(s_i)$ is therefore a function of spatial location only, which, since the rate-state equation depends only on temporal changes in pressure, may be ignored.

The other explanatory variable at our disposal is the vector of monthly production figures at the production wells, which can be smoothed out over the field [11]. We model their influence on the earthquake intensity function through the multiplier r_0 in (1). Specifically, with Δ equal to one year, write $V(s_i, t_j)$ for the gas extracted in the cell around s_i over the year preceding t_j and replace the constant r_0 by $\exp[\theta_1 + \theta_2 V(s_i, t_j)]$.

In summary, we obtain a Cox process Ψ with driving random measure defined by its density function

$$\Lambda(s, t) = \exp[\theta_1 + \theta_2 V(s, t)] \frac{\gamma_0}{\Gamma(s, t)} \quad (4)$$

which we discretise for computational convenience. Specifically, write $N(s_i, t_j)$ for the number of earthquakes in the cell of (s_i, t_j) . Then, conditional on $\Lambda(s_i, t_j)$, $N(s_i, t_j)$ is Poisson distributed with rate parameter $\Lambda(s_i, t_j)\Delta(s_i)\Delta$ independently of the earthquake counts in other cells. The Euler difference equation (2) can be solved explicitly, and we obtain

$$\Gamma(s_i, t_j) = \exp[\alpha X(s_i, t_j)] \left\{ \alpha \Delta \sum_{k=0}^{j-1} \exp[-\alpha X(s_i, t_k)] + \gamma_0 \exp[-\alpha X(s_i, t_0)] \right\}. \quad (5)$$

The parameters can be interpreted as follows. For positive θ_2 , an increase in production tends to increase the number of earthquakes; the real-valued parameter θ_1 is the intercept.

Mathematically, the model is well-defined for non-positive θ_2 as well but does not make practical sense. As for the classic model, $\gamma_0 > 0$ is the initial state of the stochastic difference equation. When α is positive and the pore pressure remains constant, the state variable increases over time and the earthquake hazard decreases according to Omori's law [15]. When the pore pressure changes due to gas extraction or fluid injection, for positive α , an increase in pore pressure due to fluid injection emphasises the temporal increase in the state variable and thus reduces the seismic hazard even more. A drop in pore pressure leads to a decrease in the state variable; its effect on the intensity of earthquakes depends on the combined effect of time and pressure.

4 Moments of the state variable

Since the randomness in the driving random measure (4) of our Cox process is induced by the state process Γ through (3), we investigate its first and second-moment properties first. Let Γ be defined by (5) for some s and the set of t_j , $j = 0, \dots, m$. Set $c = \exp(\alpha^2 \sigma^2)$ and define, for $i, j \in \mathbb{N}_0$, $f_{ij} = \exp[\alpha \{m(s, t_i) - m(s, t_j)\}]$. Then, for $k \in \mathbb{N}$,

$$\begin{aligned}\mathbb{E}\Gamma(s, t_k) &= c \left(\alpha \Delta \sum_{i=0}^{k-1} f_{ki} + \gamma_0 f_{k0} \right), \\ \text{Var}\Gamma(s, t_k) &= \alpha^2 \Delta^2 c^2 (c^2 - 1) \sum_{i=0}^{k-1} f_{ki}^2 + \alpha^2 \Delta^2 c^2 (c - 1) \sum_{i=0}^{k-1} \sum_{i \neq j=0}^{k-1} f_{ki} f_{kj} \\ &\quad + 2\alpha \Delta \gamma_0 c^2 f_{k0}^2 \left(c^2 - 1 + (c - 1) \sum_{i=1}^{k-1} f_{0i} \right) + \gamma_0^2 f_{k0}^2 c^2 (c^2 - 1)\end{aligned}$$

and, for $0 < k < l$,

$$\begin{aligned}\text{Cov}(\Gamma(s, t_k), \Gamma(s, t_l)) &= \alpha^2 \Delta^2 c^2 \sum_{i=0}^{k-1} \left[f_{ki} f_{li} (c - 1) - f_{li} \left(1 - \frac{1}{c} \right) \right] \\ &\quad + (2\alpha \Delta \gamma_0 + \gamma_0^2) c^2 f_{k0} f_{l0} (c - 1) - \alpha \Delta \gamma_0 c^2 f_{l0} \left(1 - \frac{1}{c} \right).\end{aligned}\quad (6)$$

When fluid is injected into a field, the pore pressure typically increases. In this case, the state variables are positively correlated, that is, $\text{Cov}(\Gamma(s, t_k), \Gamma(s, t_l)) \geq 0$ for all $k, l \in \mathbb{N}_0$.

When the pore pressure decreases, for example due to gas extraction, the picture is more varied. If $\alpha \sigma^2 > m(0)$, then $\text{Cov}(\Gamma(s, t_k), \Gamma(s, t_l)) \geq 0$ for all $k, l \in \mathbb{N}_0$. On the other hand, if $\alpha \sigma^2 < \min_{i \in \mathbb{N}_0} \{m(s, t_i) - m(s, t_{i+1})\}$, the minimal drop in pressure in between observation epochs,

$$\text{Cov}(\Gamma(s, t_k), \Gamma(t, t_l)) - (\alpha \Delta \gamma_0 + \gamma_0^2) c^2 (c - 1) f_{k0} f_{l0} \leq 0$$

for all $0 \leq k < l$. The proofs of these statements can be found in Appendix A. The following examples are illuminating.

Years							
1995–2001	179.81	177.39	174.86	172.20	169.42	166.50	163.48
2002–2008	160.32	157.05	153.65	150.13	146.49	142.72	138.82
2009–2015	134.81	130.68	126.43	122.04	117.53	112.91	108.16
2016–2021	103.28	98.29	93.17	87.94	82.56	77.08	

Table 1: Estimated pore pressure in bara on January 1st in the years 1995–2021 near the town of Slochteren, The Netherlands.

Example 1. Table 1 lists estimated pore pressure values near the town of Slochteren in the Groningen gas field in The Netherlands for January 1st, 1995–2021 [11]. The estimated standard deviation is $\hat{\sigma} = 7.17$.

Note that the pore pressure values are decreasing due to gas extraction. Since the intensity of induced earthquakes was very low in 1995, γ_0 can be considered infinite. Equation (6) then implies that the covariance matrix of the random vector $\Gamma(s, t_k)_k$ has positive entries only.

Example 2. Next, let us suppose that – in contrast to the previous example – the initial seismicity is very high, i.e. $\gamma_0 = 0$. Assume a linearly decreasing sequence of pore pressures $m(s, t_0) = 3$, $m(s, t_1) = 2$ and $m(s, t_2) = 1$ and set $\alpha = 1$. Then the covariance matrix of the random vector $(\Gamma(s, t_1), \Gamma(s, t_2))$ is readily calculated. Indeed, $\text{Var}\Gamma(s, t_1) = e^{-2}(e^{4\sigma^2} - e^{2\sigma^2})$ and $\text{Var}\Gamma(s, t_2) = (e^{-2} + e^{-4})(e^{4\sigma^2} - e^{2\sigma^2}) + 2e^{-3}(e^{3\sigma^2} - e^{2\sigma^2})$. As for the off-diagonal entry,

$$\begin{aligned} \text{Cov}(\Gamma(s, t_1), \Gamma(s, t_2)) &= \text{Cov}\left(e^{-1}e^{E(s, t_1) - E(s, t_0)}, e^{-2}e^{E(s, t_2) - E(s, t_0)} + e^{-1}e^{E(s, t_2) - E(s, t_1)}\right) \\ &= e^{2\sigma^2} \left\{ e^{-3}(e^{\sigma^2} - 1) - e^{-2}(1 - e^{-\sigma^2}) \right\} \end{aligned}$$

is negative for $\sigma^2 < 1$ and positive for $\sigma^2 > 1$.

5 Approximate moments of the rate variable

Recall that in the rate-and-state model defined in Section 3, the rate of induced earthquakes is inversely proportional to the state. Due to its form (5), the moments of $1/\Gamma(s, t_k)$ are intractable, but we can use the delta method [16] to approximate them in terms of the tractable moments of $\Gamma(s, t_k)$. Indeed, for $k = 0, 1, \dots$,

$$\mathbb{E} \left[\frac{1}{\Gamma(s, t_k)} \right] \approx \frac{1}{\mathbb{E}\Gamma(s, t_k)} + \frac{\text{Var}(\Gamma(s, t_k))}{(\mathbb{E}\Gamma(s, t_k))^3}. \quad (7)$$

Note that the approximation of the expectation of $\Gamma(s, t_k)^{-1}$ is at least as large as its ‘plug-in estimator’ $1/\mathbb{E}\Gamma(s, t_k)$.

The same approach can be used to obtain an approximation for the covariance. First,

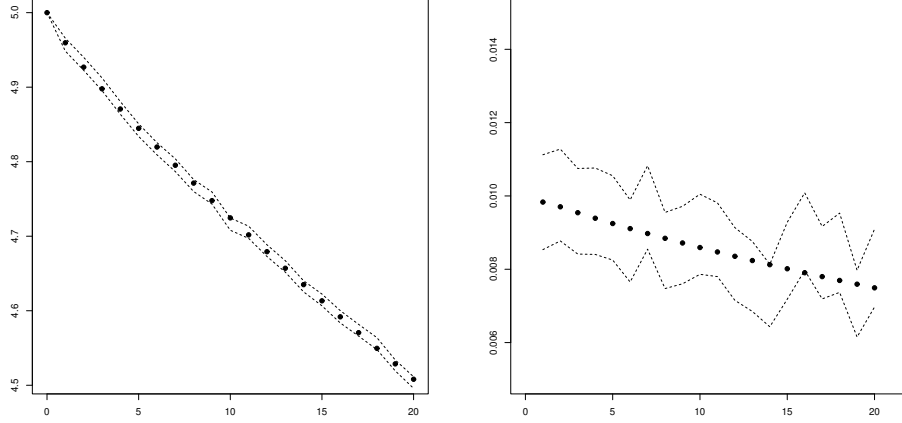


Figure 2: 95% pointwise confidence intervals for the mean (left) and variance (right) of $\Gamma(s, t_k)^{-1}$ as a function of k when $m(s, t_k) = 6 - 1/(0.5k + 1)$, $\alpha = 0.01$, $\Delta = 0.1$, $\gamma_0 = 0.2$ and $\sigma^2 = 2.0$. The dots correspond to the approximations in (7) and (8).

note that for $k, l \in \mathbb{N}_0$,

$$\begin{aligned} \mathbb{E} \left[\frac{1}{\Gamma(s, t_k)\Gamma(s, t_l)} \right] &\approx \frac{1}{\mathbb{E}[\Gamma(s, t_k)] \mathbb{E}[\Gamma(s, t_l)]} + \frac{\text{Cov}(\Gamma(s, t_k), \Gamma(s, t_l))}{(\mathbb{E}\Gamma(s, t_k))^2(\mathbb{E}\Gamma(s, t_l))^2} \\ &+ \frac{\text{Var}\Gamma(s, t_k)}{\mathbb{E}\Gamma(s, t_l)(\mathbb{E}\Gamma(s, t_k))^3} + \frac{\text{Var}\Gamma(s, t_l)}{\mathbb{E}\Gamma(s, t_k)(\mathbb{E}\Gamma(s, t_l))^3}. \end{aligned}$$

Plugging in expression (7), we obtain

$$\text{Var} \left(\frac{1}{\Gamma(s, t_k)} \right) \approx \frac{\text{Var}(\Gamma(s, t_k))}{(\mathbb{E}\Gamma(s, t_k))^4}. \quad (8)$$

For details, see Appendix B.

To investigate the accuracy of the approximations, we compare the approximation to population estimates. Recall that for an i.i.d. sample Y_1, \dots, Y_n of some random variable Y_1 with mean μ and variance σ^2 , approximate confidence intervals for μ and σ^2 take the form

$$\left(\bar{Y}_n - \frac{S_n}{\sqrt{n}} \xi_{1-\alpha/2}, \quad \bar{Y}_n + \frac{S_n}{\sqrt{n}} \xi_{1-\alpha/2} \right)$$

for μ , and

$$\left(\frac{S_n^2}{1 + \xi_{1-\alpha/2} \sqrt{\frac{2\zeta}{n-1}}}, \quad \frac{S_n^2}{1 - \xi_{1-\alpha/2} \sqrt{\frac{2\zeta}{n-1}}} \right)$$

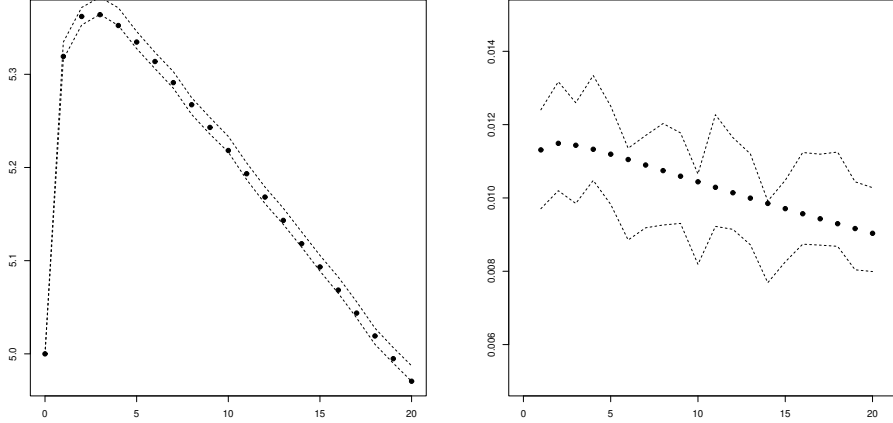


Figure 3: 95% pointwise confidence intervals for the mean (left) and variance (right) of $\Gamma(s, t_k)^{-1}$ as a function of k when $m(s, t_k) = 5 + 10/(2k + 1)$, $\alpha = 0.01$, $\Delta = 0.1$, $\gamma_0 = 0.2$ and $\sigma^2 = 2.0$. The dots correspond to the approximations in (7) and (8).

for σ^2 . Here \bar{Y}_n and S_n^2 are the sample mean and variance, and $\xi_{1-\alpha/2}$ is the $(1-\alpha/2)$ -quantile of the standard normal distribution. Furthermore, $\zeta = \frac{1}{2}(\gamma_4 - 1)$, where γ_4 denotes the ratio of the fourth central moment and the squared variance. Since γ_4 is unknown, we estimate it by $\hat{\gamma}_4 = n \sum (Y_i - m)^4 / ((n-1)^2 S_n^4)$ where m is the sample median [4]. A similar approach may be taken for the covariance, although we do not pursue it here.

We consider two cases: increasing and decreasing pore pressure. For Figure 2, define the pore pressure by the increasing function

$$m(s, t_k) = 6 - \frac{1}{1 + k/2}.$$

With parameter values $\alpha = 0.01$, $\Delta = 0.1$, $\gamma_0 = 0.2$ and $\sigma^2 = 2.0$, the 95% pointwise confidence intervals for the mean and variance are given in the left- and right-most panels. In both cases, the sample size was $n = 500$. It can be seen that the approximations are quite adequate.

For Figure 3, take the decreasing function

$$m(s, t_k) = 5 + \frac{10}{2k + 1}.$$

With the same parameter values and sample size, the 95% pointwise confidence intervals for the mean and variance are given in the left- and right-most panels. Again, the approximations are satisfactory.

6 Parameter estimation

The Cox model (4) depends on several parameters: θ_1 , θ_2 , σ^2 , α and γ_0 . The parameters γ_0 and θ_1 are not identifiable. Thus, we follow [14] and re-parametrise in terms of α/γ_0 . Recall that α and γ_0 are assumed to be positive. We therefore apply a logarithmic transformation and set $\eta = \log(\alpha/\gamma_0)$. The parameter σ^2 quantifies the uncertainty in the pore pressure observations and may be estimated by a least squares approach, and the vector of remaining parameters will be denoted by $\zeta = (\theta_1, \theta_2, \alpha, \eta)$. Since the likelihood of a Cox process is intractable [13], we use an estimating equations approach [16] for ζ .

Our inspiration is the unbiased estimating equation from [17] based on the gradient of the Poisson likelihood function. However, this method cannot be applied directly since it assumes that the intensity function λ is known analytically. For our Cox process, though,

$$\lambda(s_i, t_j) = \alpha e^{-\eta + \theta_1 + \theta_2 V(s_i, t_j)} \mathbb{E} [\Gamma(s_i, t_j)^{-1}]$$

depends on the intractable expectation of the rate variable (cf. (7)). Therefore, consider the modified estimating equation

$$F(\zeta) = \sum_{(s_i, t_j)} \frac{\nabla h(s_i, t_j; \zeta)}{h(s_i, t_j; \zeta)} \left[N(s_i, t_j) - \lambda(\widehat{s_i, t_j; \zeta}) \Delta \Delta(s_i) \right] = 0 \quad (9)$$

where

$$h(s_i, t_j; \zeta) = \frac{e^{\theta_1 + \theta_2 V(s_i, t_j)} e^{-\alpha m(s_i, t_j)}}{e^{\eta \Delta} \sum_{k=0}^{j-1} e^{-\alpha m(s_i, t_k)} + e^{-\alpha m(s_i, t_0)}}$$

and $\hat{\lambda}$ is an estimator for λ . Note that the function h is equal to the intensity function when there is no noise (i.e. $\sigma^2 = 0$), in which case (9) reduces to Poisson likelihood estimation [17]. To estimate the intensity function, we use

$$\lambda(\widehat{s_i, t_j; \zeta}) = e^{\theta_1 + \theta_2 V(s_i, t_j)} \frac{1}{L} \sum_{l=1}^L \frac{e^{-\alpha X_l(s_i, t_j)}}{e^{\eta \Delta} \sum_{k=0}^{j-1} e^{-\alpha X_l(s_i, t_k)} + e^{-\alpha X_l(s_i, t_0)}}$$

over an independent sample X_l , $l = 1, \dots, L$, of $X = m + E$. Since

$$\mathbb{E}_{\zeta} \left[N(s_i, t_j) - \lambda(\widehat{s_i, t_j; \zeta}) \Delta \Delta(s_i) \right] = \lambda(s_i, t_j; \zeta) \Delta \Delta(s_i) - \lambda(s_i, t_j; \zeta) \Delta \Delta(s_i) = 0,$$

(9) is unbiased. Equation (9) can be solved numerically.

Returning to the Groningen data (cf. Section 2.1), we discretise time in years, with t_0 equal to January 1st, 1995, and space in a 32×32 rectangular grid surrounding the gas field with s_i the centres of the cells. From [11], $\hat{\sigma} = 7.17$. For the other parameters, η is effectively $-\infty$, $\theta_1 = -5.3$, $\theta_2 = 9.7$ and $\alpha = 0.0097$ using $L = 1,000$ samples of X for $\hat{\lambda}$.

The quality of an estimating equation is expressed in terms of the variance of $F(\zeta_0)$ under the true value ζ_0 of the parameter vector. However, since multiplying the left- and right-hand side of (9) by the same constant does not alter the estimator but does affect the variance, one needs to fix the scale by $U = -\mathbb{E}_{\zeta_0} J_F(\zeta_0)$, the expectation of the negative Jacobian [7, 8].

The variance of the scaled estimating equation is known as the inverse Godambe matrix. We refer to Appendix C for explicit expressions of $F(\zeta)$ and its Jacobian, to Appendix D for an asymptotic expression of the Godambe matrix when the discretisation mesh goes to zero.

Under an appropriate asymptotic scheme, for example by letting the discretisation get finer and finer, the observation window larger and larger, the inverse Godambe matrix can be interpreted as the variance of $\hat{\zeta}$. However, for the Groningen data, in view of the small earthquake counts and numerical stability considerations, we discretise rather coarsely. Therefore it is better to use a parametric bootstrap approach [16] to obtain approximate confidence intervals. This way, at 95% confidence level, we obtained the confidence interval $(-5.6, -5.1)$ for θ_1 , $(7.0, 12.8)$ for θ_2 and $(0.006, 0.01)$ for α . Note that the confidence interval for θ_2 contains only strictly positive values, indicating that an increase in production leads to a higher earthquake hazard the next year.

We also need to validate our model. To do so, consider the Pearson residuals

$$\frac{n(s_i, t_j) - \lambda(s_i, t_j; \hat{\zeta})\Delta\Delta(s_i)}{\sqrt{\hat{\lambda}(s_i, t_j; \hat{\zeta})\Delta\Delta(s_i) + \lambda(s_i, t_j; \hat{\zeta})^2(e^{4\hat{\alpha}^2\hat{\sigma}^2} - 1)\Delta^2\Delta(s_i)^2}}$$

for $t_j > t_0$ and all s_i . Because the observed incidences take only very small values, residual plots are not helpful in assessing the model fit. A better alternative is to divide the data into bins based on their fitted values and plot the average residuals against the average fitted value for each bin, as shown in Figure 4. The fit seems to be adequate for most bins.

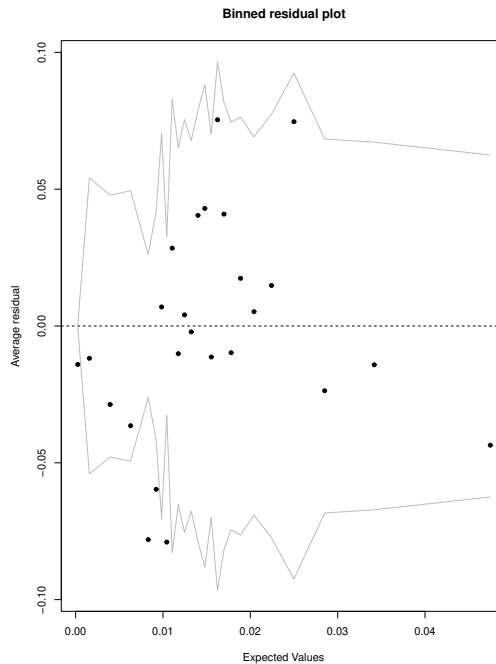


Figure 4: Average Pearson residual against average fitted value for 25 bins for model (10). The grey lines correspond to two standard deviations bounds.

To summarise, after excluding η , our final model is a log-Gaussian Cox process with driving random measure

$$\Delta\Delta(s_i) \exp[\theta_1 + \theta_2 V(s_i, t_j) + \alpha(X(s_i, t_0) - X(s_i, t_j))]. \quad (10)$$

It is interesting to observe that a purely temporal analysis [1] yielded a similar model with a time component instead of a drop in pore pressure.

7 Monitoring seismic hazard

Monitoring is based on the posterior distribution of Λ or, equivalently, E given the recorded earthquakes. Write $\mathbf{n} = (n(s_i, t_j))_{i,j}$ for the vector of observed earthquake counts $n(s_i, t_j)$ in the cells indexed by the s_i and t_j . Then, upon ignoring all terms that do not depend on E , the log posterior likelihood reads

$$\log f(e(s_i, t_j)_{i,j} | \mathbf{n}) = - \sum_{(s_i, t_j)} \frac{e(s_i, t_j)^2}{2\sigma^2} + \sum_{(s_i, t_j)} \{n(s_i, t_j) \log \Lambda_e(s_i, t_j) - \Delta\Delta_S \Lambda_e(s_i, t_j)\} \quad (11)$$

where the s_i range through the cell representatives in W_S and t_j indicate the time intervals. We write Λ_e to emphasise the dependence of (4) on the realisation e of E . The marginal posterior likelihood for fixed s_i will be denoted by $f_{s_i}(e(s_i, t_j)_j | \mathbf{n})$.

We use a Markov chain Monte Carlo technique, the Metropolis adjusted Langevin algorithm (MALA) proposed by Julian Besag [2], to draw samples from (11). The algorithm is a Metropolis–Hastings sampler [12] in which moves are proposed in the direction of the gradient of (11). It is important to observe that the independence of our model across the spatial domain allows for parallel implementation. Thus, for each spatial grid cell around s , we run the following algorithm for $e(s, t_0), \dots, e(s, t_m)$.

Algorithm 1. *If the current state is $\mathbf{e}(s) = (e(s, t_0), \dots, e(s, t_m))$ and the earthquake count vector is \mathbf{n} , then*

1. *sample a realisation $\tilde{e}(s, t_0), \dots, \tilde{e}(s, t_m)$ from independent normal distributions with variance h and mean*

$$\mu(s, t_j; e) = \left(1 - \frac{h}{2\sigma^2}\right) e(s, t_j) - \frac{h}{2}\alpha \{n(s, t_j) - \Lambda_e(s, t_j)\Delta\Delta(s)\}$$

for $j > 0$ and

$$\mu(s, t_0; e) = \left(1 - \frac{h}{2\sigma^2}\right) e(s, t_0) + \frac{h}{2}\alpha \sum_{i=1}^m \{n(s, t_i) - \Lambda_e(s, t_i)\Delta\Delta(s)\};$$

2. *accept the new state with probability*

$$\frac{f_s(\tilde{e}(s, t_0), \dots, \tilde{e}(s, t_m) | \mathbf{n}) \exp(-\sum_{j=0}^m (e(s, t_j) - \mu(s, t_j; \tilde{e}))^2 / (2h))}{f_s(e(s, t_0), \dots, e(s, t_m) | \mathbf{n}) \exp(-\sum_{j=0}^m (\tilde{e}(s, t_j) - \mu(s, t_j; e))^2 / (2h))}.$$

Since the proposals are governed by a normal distribution, which has a strictly positive probability density, by [12, Lemma 1.1], the Markov chain generated by the MALA algorithm above is f_s -irreducible. Also f_s is a strictly positive probability density on \mathbb{R}^m , so by [12, Lemma 1.2] the Markov chain is also aperiodic. By construction, f_s is an invariant measure. We conclude that the Markov chain converges in total variation from almost all initial states [13, Proposition 7.7].

Having obtained samples from the posterior distribution of Λ , we are ready to monitor earthquake hazard. Monitoring targets the posterior distribution of counts in the time interval $[t_{m+1}, t_{m+1} + \Delta]$, that is, in the year 2022. For our Groningen data, recalling (10), these counts follow a Poisson distribution with intensity

$$\exp \left[\hat{\theta}_0 + \hat{\theta}_1 V(s, t_m + \Delta) + \hat{\alpha} \{X_i(s, t_0) - m(s, t_m + \Delta) - E_i(s, t_m + \Delta)\} \right] \times \Delta \Delta(s)$$

where the family $\{X_i(s, t_0) = m(s, t_0) + E_i(s, t_0)\}_{i=1, \dots, I}$ indexed by cell representatives s use the samples $E_i(s, t_0)$ from the posterior given the counts generated by the MALA algorithm above, and $E_i(s, t_m + \Delta)$ is white noise with variance $\hat{\sigma}^2$.

With $h = 0.02\hat{\sigma}$, a burn-in of 10,000 steps for each spatial grid cell and subsampling every 1,000 steps, we plot the mean and standard deviation of $\Lambda(s, t_m + \Delta)\Delta\Delta(s)$, intensity of earthquakes in each spatial cell around s for the year 2022, in the bottom row of Figure 5. The top row in the same figure depicts the covariates, namely the gas production figures in the preceding year and the estimated drop in pressure up to 2022. We show the histogram of earthquake counts for a sample of size $I = 5,000$ in Figure 6.

The total volume of gas extracted in 2021 was low, 6.48 Nbcm compared to around over 50 Nbcm in 2013, and concentrated in the south of the gas field. As for the pressure, it can be seen that the estimated decrease in pressure is smallest in the western and eastern periphery. Because the wells in the south were taken into production earlier than those in the north, initially a larger drop in pressure was measured in the south. To reduce this imbalance somewhat, in the seventies, eighties and nineties, the northern locations were preferred for production. However, in response to concerns following a major earthquake, the Dutch government imposed production caps on some northern clusters in 2014, which again emphasised the larger drop in pore pressure in the south. Additionally, the top-right plot in Figure 5 shows a larger estimated fall in pressure in the far north offshore part of the field. Indeed, the observation well at Oldorp in the north-western corner of the field is known to be atypical for the field: quite high values were observed in 1995 and there are very few recent measurements. We refer to [9] for a more detailed description of the geology of the Groningen field.

The risk map in the lower left panel of Figure 5 reflects these features. The area of increased risk due to gas extraction in the south of the field is tilted according to the pore pressure gradient, there is a smaller risk in the peripheral regions and the absence of production in the far north offsets the large drop in pressure. The standard deviation of the posterior is highest in the large production region in the southeast and in the offshore northern region.

We also plot the histogram of the posterior earthquake count over 2022. For comparison, the actual number of earthquakes was 12.

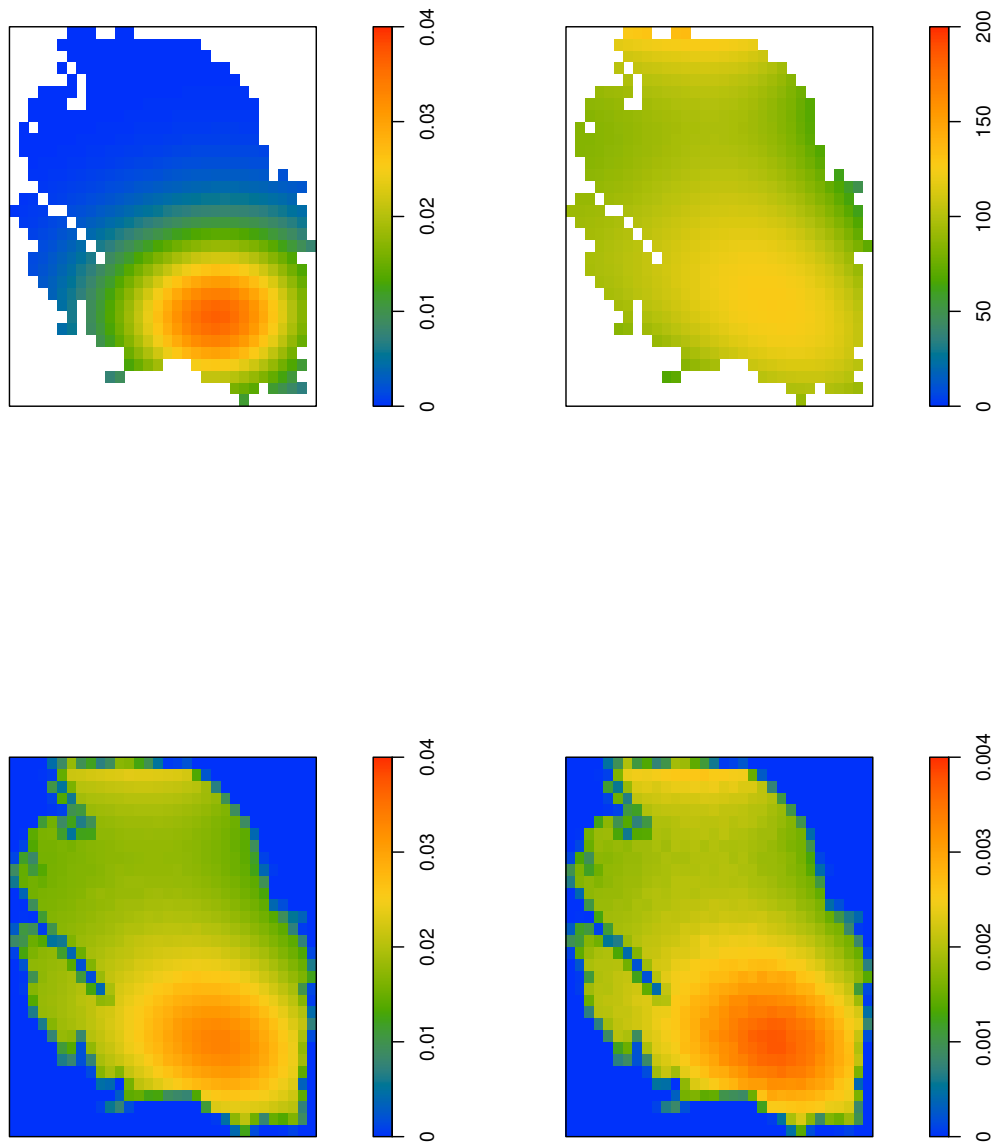


Figure 5: Top left: Smoothed gas production over 2021 (in Nbcm for each grid cell). Top right: Estimated pressure drop (in bara for each grid cell) from 1995 until 2022. Bottom left: Mean posterior number of earthquakes in 2022 (for each grid cell, sample size $I = 5,000$). Bottom right: Sample standard deviation of posterior number of earthquakes in 2022 (for each grid cell, sample size $I = 5,000$).

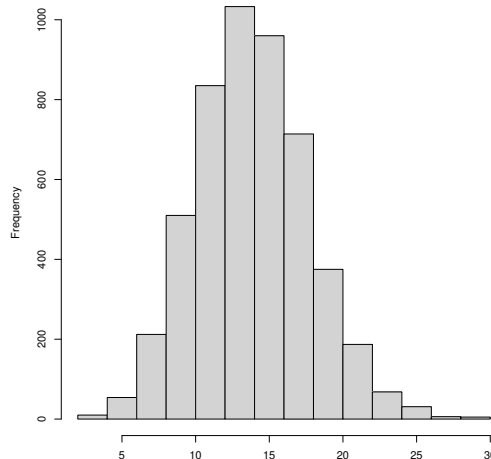


Figure 6: Histogram of a sample of size $I = 5,000$ from the posterior distribution of the number of earthquakes in 2022.

8 Conclusion

In this paper, we explored the seismic risk in the Groningen gas field by modifying the state-of-the-art rate-state model in two directions, namely allowing for noise in pore pressure measurements and explicitly taking into account gas production volumes. We investigated the first- and second-moment measures of the resulting Cox process and estimated its parameters by a tailor-made estimating equation. We then constructed a Markov Chain Monte-Carlo algorithm to monitor seismicity.

An important feature of our approach is that it is completely data-driven and does not rely on reservoir models. The advantage of working in a data-driven fashion is that erroneous model assumptions cannot impact the monitoring and that uncertainty quantification is part of the toolbox; a drawback is that the accuracy depends on the quality of the data at hand. In our context, from the mid 1990s, the earthquake catalogue maintained by the Royal Netherlands Meteorological Office (KNMI) is accurate. Production figures too are available at various public websites, but not always accurate. Therefore we used the data provided directly by the production company NAM for best results. Pore pressure measurements, however, are available only at wells and are quite sparse. Especially in recent years, there are not many observations. In view of the facts that caps on production were put in place in 2014 and that production stopped altogether in 2024, which will likely affect the future

drop in pore pressure, we recommend stepping up efforts in pore pressure measurements to improve the monitoring of seismic hazard.

The model can be extended in various directions. For instance, other explanatory variables, such as information on fault lines and subsidence, or other geological features of the field, could be taken into account. Also, spatially correlated random factors could be added to the model. From a theoretical point of view, an asymptotic theory for the estimating equation would be of interest. Finally, we intend to compare our data-driven approach with one that inputs the NAM reservoir model for the pore pressure.

Acknowledgements

This research was funded by the Dutch Research Council NWO through their DEEPNL programme (grant number DEEP.NL.2018.033). We are grateful to Mr Van Eijs for providing us with data on gas production.

References

- [1] Baki, Z., Lieshout, M.N.M. van (2022). The influence of gas production on seismicity in the Groningen field. *Proceedings of the 10th International Workshop on Spatio-Temporal Modelling*, C. Comas and J. Mateu (Eds.), 163–167.
- [2] Besag, J. (1994). Discussion to Grenander and Miller, Representations of knowledge in complex systems. *Journal of the Royal Statistical Society B* 56:549–603.
- [3] Candela, T. et al. (2019). Depletion-induced seismicity at the Groningen gas field: Coulomb rate-and-state models including differential compaction effect. *Journal of Geophysical Research: Solid Earth* 124:7081–7104.
- [4] Curto, J.D. (2023). Confidence intervals for means and variances of non-normal distributions. *Communications in Statistics – Simulation and Computation* 52:4414–4430.
- [5] Chiu, S.N., Stoyan, D., Kendall, W.S., Mecke, J. (2013). *Stochastic geometry and its applications*. Wiley, 3rd ed.
- [6] Dempsey, D., Suckale, J. (2017). Physics-based forecasting of induced seismicity at Groningen gas field, the Netherlands. *Geophysical Research Letters* 22:7773–7782.
- [7] Godambe, V.P. (1985). The foundations of finite sample estimation in stochastic processes. *Biometrika* 72:419–428.
- [8] Godambe, V.P., Heyde, C.C. (2010). *Quasi-likelihood and optimal estimation*. Pages 386–399 in: *Selected works of C.C. Heyde*. Springer.
- [9] Jager, J. de, Visser, C. (2017). Geology of the Groningen field—an overview. *Netherlands Journal of Geosciences* 96:3–15.

- [10] Kühn, D., Hainzl, S., Dahm, T., Richter, G., Vera Rodriguez, I. (2022). A review of source models to further the understanding of the seismicity of the Groningen field. *Netherlands Journal of Geosciences*, 101:e11.
- [11] Lieshout, M.N.M. van, Baki, Z. (2024). Exploring seismic hazard in the Groningen gas field using adaptive kernel smoothing. *Mathematical Geosciences* 56:1185–1206.
- [12] Mengersen, K.L, Tweedie, R.L. (1996). Rates of convergence of the Hastings and Metropolis algorithms. *The Annals of Statistics* 24:101–121.
- [13] Møller, J., Waagepetersen, R.P. (2004). *Statistical inference and simulation for spatial point processes*. Chapman & Hall.
- [14] Richter, G., Hainzl, S., Dahm, T., Zöller, G. (2020). Stress-based statistical modeling of the induced seismicity at the Groningen gas field, The Netherlands. *Environmental Earth Sciences* 79, 252.
- [15] Utsu, T., Ogata, Y., Matsu'ura, R.S. (1995). The centenary of the Omori formula for a decay law of aftershock activity. *Journal of Physics of the Earth* 43:1–33.
- [16] Vaart, A.W. van der (1998). *Asymptotic statistics*. Cambridge University Press.
- [17] Waagepetersen, R.P. (2007). An estimating function approach to inference for inhomogeneous Neyman–Scott processes. *Biometrics* 63:252–258.

Appendix A: Calculation of $\mathbb{E}\Gamma(s, t_k)$ and $\text{Cov}(\Gamma(s, t_k), \Gamma(s, t_l))$

Since

$$\mathbb{E}e^{tZ} = \exp(\mu t + \sigma^2 t^2/2)$$

when Z is normally distributed with mean μ and variance σ^2 , the formula for $\mathbb{E}\Gamma(s, t_k)$ in Section 4 follows immediately. Moreover, for $0 < k \leq l$,

$$\begin{aligned} \text{Cov}(\Gamma(s, t_k), \Gamma(s, t_l)) &= \alpha^2 \Delta^2 \sum_{i=0}^{k-1} \sum_{j=0}^{l-1} \text{Cov}\left(e^{\alpha[X(s, t_k) - X(s, t_i)]}, e^{\alpha[X(s, t_l) - X(s, t_j)]}\right) \\ &+ \alpha \Delta \gamma_0 \sum_{i=0}^{k-1} \text{Cov}\left(e^{\alpha[X(s, t_k) - X(s, t_i)]}, e^{\alpha[X(s, t_l) - X(s, t_0)]}\right) \\ &+ \alpha \Delta \gamma_0 \sum_{j=0}^{l-1} \text{Cov}\left(e^{\alpha[X(s, t_k) - X(s, t_0)]}, e^{\alpha[X(s, t_l) - X(s, t_j)]}\right) \\ &+ \gamma_0^2 \text{Cov}\left(e^{\alpha[X(s, t_k) - X(s, t_0)]}, e^{\alpha[X(s, t_l) - X(s, t_0)]}\right). \end{aligned} \quad (12)$$

Let us work out the terms in the expression on the right-hand side of equation (12) one by one. First, consider the double sum over i and j . Because of the independence of the components of the random vector E , summands for which k, l, i and j are all different do not contribute. Therefore, for $0 < k = l$, the total contribution of the double sum is

$$\alpha^2 \Delta^2 c^2 \sum_{i=0}^{k-1} f_{ki}^2 (c^2 - 1) + \alpha^2 \Delta^2 c^2 \sum_{i=0}^{k-1} f_{ki} \sum_{j \neq i; j=0}^{k-1} f_{kj} (c - 1).$$

For $0 < k < l$, the double sum contributes non-zero entries for $i = j$ (which cannot be equal to k or l) and for $i \neq j = k$. Their total contribution is

$$\alpha^2 \Delta^2 c^2 \sum_{i=0}^{k-1} f_{ki} f_{li} (c - 1) - \alpha^2 \Delta^2 c^2 \sum_{i=0}^{k-1} f_{li} \left(1 - \frac{1}{c}\right).$$

Next consider the two single sums on the right-hand side of (12). If $0 < k = l$, they are identical and each one is equal to

$$\alpha \Delta \gamma_0 c^2 \left[f_{k0}^2 (c^2 - 1) + (c - 1) \sum_{i=1}^{k-1} f_{ki} f_{k0} \right].$$

In the case that $0 < k < l$, the sum over i has a non-zero contribution only for $i = 0$, and the sum over j has non-vanishing contributions for $j = 0$ and $j = k$. Adding these up, we obtain

$$\alpha \Delta \gamma_0 c^2 f_{l0} \left[2f_{k0} (c - 1) - \left(1 - \frac{1}{c}\right) \right].$$

Finally, the last term in the expression on the right-hand side of equation (12) reads $\gamma_0^2 f_{k0}^2 c^2 (c^2 - 1)$ for $0 < k = l$ and $\gamma_0^2 f_{k0} f_{l0} c^2 (c - 1)$ when $0 < k < l$. Expression (6) now follows

from tallying up the various contributions. The variance of the state variable is obtained by taking $k = l$.

When the pore pressure increases, the state variables are non-negatively correlated. To see this, consider $0 \leq i < k < l$. Then

$$\alpha^2 \Delta^2 f_{li} \{f_{ki} c^2 (c-1) - c(c-1)\} \geq 0$$

if $\sigma^2 = 0$ or $cf_{ki} \geq 1$. The latter condition is equivalent to

$$\alpha^2 \sigma^2 + \alpha \{m(s, t_k) - m(s, t_i)\} \geq 0$$

and is implied by the assumption that m is increasing. By the same argument, for increasing pore pressure, $\alpha \Delta \gamma_0 f_{l0} \{f_{k0} c^2 (c-1) - c(c-1)\} \geq 0$ and an appeal to (6) completes the proof.

Next, suppose that the pore pressure decreases. For $0 \leq i < k < l$, consider $\alpha^2 \Delta^2 f_{li} c (c-1) \{cf_{ki} - 1\}$. The term in between curly brackets is negative if and only if

$$\alpha \{m(s, t_k) - m(s, t_i)\} + \alpha^2 \sigma^2 < 0.$$

Since m is decreasing, if $\alpha \sigma^2 < \min_i \{m(s, t_i) - m(s, t_{i+1})\}$,

$$\alpha^2 \sigma^2 < m(s, t_i) - m(s, t_{i+1}) \leq m(s, t_i) - m(s, t_k)$$

so that $\alpha^2 \Delta^2 f_{li} c (c-1) \{cf_{ki} - 1\} \leq 0$. Since the same argument can be used to show that $\alpha \Delta \gamma_0 f_{l0} c (c-1) \{cf_{k0} - 1\} \leq 0$,

$$\text{Cov}(\Gamma(s, t_k), \Gamma(t, t_l)) - (\alpha \Delta \gamma_0 + \gamma_0^2) c^2 (c-1) f_{k0} f_{l0} \leq 0.$$

If $\alpha \sigma^2 > m(0)$, then

$$\alpha^2 \sigma^2 > m(s, t_0) \geq m(s, t_i) \geq m(s, t_i) - m(s, t_k)$$

and therefore $\alpha^2 \Delta^2 f_{li} c (c-1) \{cf_{ki} - 1\} \geq 0$. Similarly, $\alpha \Delta \gamma_0 f_{l0} c (c-1) \{cf_{k0} - 1\} \geq 0$. Consequently, $\text{Cov}(\Gamma(s, t_k), \Gamma(t, t_l)) \geq 0$.

Appendix B: Approximate momens of the rate variable

To approximate the expectation of $1/\Gamma(s, t_k)$, apply the delta method based on the Taylor expansion

$$\frac{1}{x_0 + h} \approx \frac{1}{x_0} - \frac{h}{x_0^2} + \frac{1}{2!} \frac{2h^2}{x_0^3}$$

around x_0 equal to the expectation of $\Gamma(s, t_k)$. Upon taking the expectation, one obtains that

$$\mathbb{E} \left[\frac{1}{\Gamma(s, t_k)} \right] \approx \frac{1}{\mathbb{E}\Gamma(s, t_k)} - \mathbb{E} \left[\frac{\Gamma(s, t_k) - \mathbb{E}\Gamma(s, t_k)}{(\mathbb{E}\Gamma(s, t_k))^2} \right] + \mathbb{E} \left[\frac{(\Gamma(s, t_k) - \mathbb{E}\Gamma(s, t_k))^2}{(\mathbb{E}\Gamma(s, t_k))^3} \right].$$

The middle term on the right-hand side is zero, and (7) follows.

The Taylor expansion of the function $(x, y) \mapsto 1/(xy)$ around the point $(\mathbb{E}\Gamma(s, t_k), \mathbb{E}\Gamma(s, t_l))$ yields the approximation

$$\begin{aligned} \frac{1}{\Gamma(s, t_k)} \frac{1}{\Gamma(s, t_l)} &\approx \frac{1}{\mathbb{E}\Gamma(s, t_k)} \frac{1}{\mathbb{E}\Gamma(s, t_l)} + \frac{(\Gamma(s, t_k) - \mathbb{E}\Gamma(s, t_k)) (\Gamma(s, t_l) - \mathbb{E}\Gamma(s, t_l))}{(\mathbb{E}\Gamma(s, t_k))^2 (\mathbb{E}\Gamma(s, t_l))^2} \\ &- \frac{\Gamma(s, t_k) - \mathbb{E}\Gamma(s, t_k)}{(\mathbb{E}\Gamma(s, t_k))^2 \mathbb{E}\Gamma(s, t_l)} - \frac{\Gamma(s, t_l) - \mathbb{E}\Gamma(s, t_l)}{(\mathbb{E}\Gamma(s, t_l))^2 \mathbb{E}\Gamma(s, t_k)} \\ &+ \frac{(\Gamma(s, t_k) - \mathbb{E}\Gamma(s, t_k))^2}{(\mathbb{E}\Gamma(s, t_k))^3 \mathbb{E}\Gamma(s, t_l)} + \frac{(\Gamma(s, t_l) - \mathbb{E}\Gamma(s, t_l))^2}{\mathbb{E}\Gamma(s, t_k) (\mathbb{E}\Gamma(s, t_l))^3} \end{aligned}$$

up to second-order moments. Finally take expectations to obtain an approximation of the expected cross product of the rate.

Appendix C: Partial derivatives for parameter estimation

Write, for $s \in W_S$ the centre of a cell with area $\Delta(s)$ and $t_k = t_0 + k\Delta$,

$$S(s, t_k) = e^\eta \Delta \sum_{i=0}^{k-1} e^{-\alpha(m(s, t_i) - m(s, t_k))} + e^{-\alpha(m(s, t_0) - m(s, t_k))}$$

and let h be as in Section 6. Then $\frac{\partial}{\partial \theta_1} h(s, t_k) / h(s, t_k) = 1$ and

$$\frac{\frac{\partial}{\partial \theta_2} h(s, t_k)}{h(s, t_k)} = V(s, t_k), \quad \frac{\frac{\partial}{\partial \alpha} h(s, t_k)}{h(s, t_k)} = -\frac{\frac{\partial}{\partial \alpha} S(s, t_k)}{S(s, t_k)}, \quad \frac{\frac{\partial}{\partial \eta} h(s, t_k)}{h(s, t_k)} = -\frac{\frac{\partial}{\partial \eta} S(s, t_k)}{S(s, t_k)}.$$

These derivatives define F_ζ in the estimating equation (9). The partial derivatives of S can be calculated recursively:

$$\begin{aligned} S(s, t_k) &= (S(s, t_{k-1}) + e^\eta \Delta) e^{-\alpha(m(s, t_{k-1}) - m(s, t_k))} \\ \frac{\partial}{\partial \alpha} S(s, t_k) &= \left(\frac{\partial}{\partial \alpha} S(s, t_{k-1}) \right) e^{-\alpha(m(s, t_{k-1}) - m(s, t_k))} - (m(s, t_{k-1}) - m(s, t_k)) S(s, t_k) \\ \frac{\partial}{\partial \eta} S(s, t_k) &= \left(\frac{\partial}{\partial \eta} S(s, t_{k-1}) + e^\eta \Delta \right) e^{-\alpha(m(s, t_{k-1}) - m(s, t_k))} \\ \frac{\partial^2}{\partial \alpha^2} S(s, t_k) &= \left(\frac{\partial^2}{\partial \alpha^2} S(s, t_{k-1}) \right) e^{-\alpha(m(s, t_{k-1}) - m(s, t_k))} \\ &\quad - (m(s, t_{k-1}) - m(s, t_k)) \left[\frac{\partial}{\partial \alpha} S(s, t_k) + \left(\frac{\partial}{\partial \alpha} S(s, t_{k-1}) \right) e^{-\alpha(m(s, t_{k-1}) - m(s, t_k))} \right] \\ \frac{\partial^2}{\partial \alpha \partial \eta} S(s, t_k) &= \left(\frac{\partial^2}{\partial \alpha \partial \eta} S(s, t_{k-1}) \right) e^{-\alpha(m(s, t_{k-1}) - m(s, t_k))} - (m(s, t_{k-1}) - m(s, t_k)) \frac{\partial}{\partial \eta} S(s, t_k) \end{aligned}$$

and $\frac{\partial^2}{\partial \eta^2} S(s, t_k) = \frac{\partial}{\partial \eta} S(s, t_k)$.

Equation (9) may be solved by the Newton method that iteratively solves the equation

$$J_F(\zeta_n)(\zeta_{n+1} - \zeta_n) = -F(\zeta_n)$$

for $\zeta_{n+1} - \zeta_n$. The Jacobian $J_F(\zeta)$ is a four-by-four matrix with components

$$\begin{array}{l|l} J_F(\zeta)_{1,1} = -\sum_{(s_i, t_j)} \widehat{\lambda}(s_i, t_j) \Delta \Delta(s_i) & J_F(\zeta)_{2,1} = -\sum_{(s_i, t_j)} V(s_i, t_j) \widehat{\lambda}(s_i, t_j) \Delta \Delta(s_i) \\ J_F(\zeta)_{1,2} = -\sum_{(s_i, t_j)} V(s_i, t_j) \widehat{\lambda}(s_i, t_j) \Delta \Delta(s_i) & J_F(\zeta)_{2,2} = -\sum_{(s_i, t_j)} V(s_i, t_j)^2 \widehat{\lambda}(s_i, t_j) \Delta \Delta(s_i) \\ J_F(\zeta)_{1,3} = -\sum_{(s_i, t_j)} \frac{\partial \widehat{\lambda}(s_i, t_j)}{\partial \alpha} \Delta \Delta(s_i) & J_F(\zeta)_{2,3} = -\sum_{(s_i, t_j)} V(s_i, t_j) \frac{\partial \widehat{\lambda}(s_i, t_j)}{\partial \alpha} \Delta \Delta(s_i) \\ J_F(\zeta)_{1,4} = -\sum_{(s_i, t_j)} \frac{\partial \widehat{\lambda}(s_i, t_j)}{\partial \eta} \Delta \Delta(s_i) & J_F(\zeta)_{2,4} = -\sum_{(s_i, t_j)} V(s_i, t_j) \frac{\partial \widehat{\lambda}(s_i, t_j)}{\partial \eta} \Delta \Delta(s_i) \\ \\ J_F(\zeta)_{3,1} = \sum_{(s_i, t_j)} \frac{\frac{\partial S(s_i, t_j)}{\partial \alpha}}{S(s_i, t_j)} \widehat{\lambda}(s_i, t_j) \Delta \Delta(s_i) & J_F(\zeta)_{3,2} = \sum_{(s_i, t_j)} \frac{\frac{\partial S(s_i, t_j)}{\partial \alpha}}{S(s_i, t_j)} V(s_i, t_j) \widehat{\lambda}(s_i, t_j) \Delta \Delta(s_i) \\ J_F(\zeta)_{4,1} = \sum_{(s_i, t_j)} \frac{\frac{\partial S(s_i, t_j)}{\partial \eta}}{S(s_i, t_j)} \widehat{\lambda}(s_i, t_j) \Delta \Delta(s_i) & J_F(\zeta)_{4,2} = \sum_{(s_i, t_j)} \frac{\frac{\partial S(s_i, t_j)}{\partial \eta}}{S(s_i, t_j)} V(s_i, t_j) \widehat{\lambda}(s_i, t_j) \Delta \Delta(s_i). \end{array}$$

In none of these the counts play a role. They do for the last two terms in the third row:

$$\sum_{(s_i, t_j)} \left\{ \left(\frac{\partial S(s_i, t_j)}{\partial \alpha} \right)^2 - \frac{\partial^2 S(s_i, t_j)}{\partial \alpha^2} \right\} [N(s_i, t_j) - \hat{\lambda}(s_i, t_j) \Delta \Delta(s_i)] +$$

$$\sum_{(s_i, t_j)} \frac{\partial S(s_i, t_j)}{S(s_i, t_j)} \frac{\partial \hat{\lambda}(s_i, t_j)}{\partial \alpha} \Delta \Delta(s_i)$$

and

$$\sum_{(s_i, t_j)} \left\{ \frac{\partial S(s_i, t_j)}{\partial \alpha} \frac{\partial S(s_i, t_j)}{\partial \eta} - \frac{\partial^2 S(s_i, t_j)}{\partial \alpha \partial \eta} \right\} [N(s_i, t_j) - \hat{\lambda}(s_i, t_j) \Delta \Delta(s_i)] +$$

$$\sum_{(s_i, t_j)} \frac{\partial S(s_i, t_j)}{S(s_i, t_j)} \frac{\partial \hat{\lambda}(s_i, t_j)}{\partial \eta} \Delta \Delta(s_i).$$

Finally, the two last entries of the fourth row are

$$\sum_{(s_i, t_j)} \left\{ \frac{\partial S(s_i, t_j)}{\partial \alpha} \frac{\partial S(s_i, t_j)}{\partial \eta} - \frac{\partial^2 S(s_i, t_j)}{\partial \alpha \partial \eta} \right\} [N(s_i, t_j) - \hat{\lambda}(s_i, t_j) \Delta \Delta(s_i)] +$$

$$\sum_{(s_i, t_j)} \frac{\partial S(s_i, t_j)}{S(s_i, t_j)} \frac{\partial \hat{\lambda}(s_i, t_j)}{\partial \alpha} \Delta \Delta(s_i)$$

and

$$\sum_{(s_i, t_j)} \left\{ \left(\frac{\partial S(s_i, t_j)}{\partial \eta} \right)^2 - \frac{\partial^2 S(s_i, t_j)}{\partial \eta^2} \right\} [N(s_i, t_j) - \hat{\lambda}(s_i, t_j) \Delta \Delta(s_i)] +$$

$$\sum_{(s_i, t_j)} \frac{\partial S(s_i, t_j)}{S(s_i, t_j)} \frac{\partial \hat{\lambda}(s_i, t_j)}{\partial \eta} \Delta \Delta(s_i).$$

Note that the Jacobian is not symmetric as it does not correspond to a likelihood! A recursive formula for the partial derivatives of S is given above. It remains to calculate the partial derivatives of $\hat{\lambda}$. Those with respect to θ_1 and θ_2 are, respectively, $\hat{\lambda}$ and $V\hat{\lambda}$. Furthermore,

$$\frac{\partial \hat{\lambda}(s, t_k)}{\partial \alpha} = e^{\theta_1 + \theta_2 V(s, t_k)} \frac{1}{L} \sum_{l=1}^L \frac{-\frac{\partial}{\partial \alpha} S_{X_l}(s, t_k)}{S_{X_l}(s, t_k)^2}$$

$$\frac{\partial \hat{\lambda}(s, t_k)}{\partial \eta} = e^{\theta_1 + \theta_2 V(s, t_k)} \frac{1}{L} \sum_{l=1}^L \frac{-\frac{\partial}{\partial \eta} S_{X_l}(s, t_k)}{S_{X_l}(s, t_k)^2}$$

with

$$\begin{aligned}
S_{X_l}(s, t_k) &= e^\eta \Delta \sum_{i=0}^{k-1} e^{-\alpha(X_l(s, t_i) - X_l(s, t_k))} + e^{-\alpha(X_l(s, t_0) - X_l(s, t_k))} \\
\frac{\partial}{\partial \alpha} S_{X_l}(s, t_k) &= -(X_l(s, t_0) - X_l(s, t_k)) e^{-\alpha(X_l(s, t_0) - X_l(s, t_k))} \\
&\quad - e^\eta \Delta \sum_{i=0}^{k-1} (X_l(s, t_i) - X_l(s, t_k)) e^{-\alpha(X_l(s, t_i) - X_l(s, t_k))} \\
\frac{\partial}{\partial \eta} S_{X_l}(s, t_k) &= e^\eta \Delta \sum_{i=0}^{k-1} e^{-\alpha(X_l(s, t_i) - X_l(s, t_k))}.
\end{aligned}$$

Appendix D: Godambe matrix

The Godambe matrix of the estimating equation (9) with $e^\eta = 0$ and remaining parameter vector $\zeta = (\theta_1, \theta_2, \alpha)$ is of the form $U\Sigma_F^{-1}U$. In the limit upon letting Δ and all $\Delta(s)$ go to zero, the first two columns of U read

$$\begin{bmatrix} \int_{W_S \times W_T} \lambda(s, t; \zeta) ds dt & \int_{W_S \times W_T} V(s, t) \lambda(s, t; \zeta) ds dt \\ \int_{W_S \times W_T} V(s, t) \lambda(s, t; \zeta) ds dt & \int_{W_S \times W_T} V(s, t)^2 \lambda(s, t; \zeta) ds dt \\ \int_{W_S \times W_T} (m(s, t_0) - m(s, t)) \lambda(s, t; \zeta) ds dt & \int_{W_S \times W_T} (m(s, t_0) - m(s, t)) V(s, t) \lambda(s, t; \zeta) ds dt \end{bmatrix}$$

for

$$\lambda(s, t; \zeta) = \exp [\theta_1 + \theta_2 V(s, t) + \alpha(m(s, t_0) - m(s, t)) + \alpha^2 \sigma^2].$$

The last column of U is

$$\begin{bmatrix} \int_{W_S \times W_T} l(s, t; \zeta) ds dt \\ \int_{W_S \times W_T} V(s, t) l(s, t; \zeta) ds dt \\ \int_{W_S \times W_T} (m(s, t_0) - m(s, t)) l(s, t; \zeta) ds dt \end{bmatrix} \quad (13)$$

where

$$l(s, t; \zeta) = \mathbb{E}_\zeta \left\{ (X(s, t_0) - X(s, t)) e^{\theta_1 + \theta_2 V(s, t)} e^{\alpha(X(s, t_0) - X(s, t))} \right\}.$$

The first two columns of the matrix Σ_F are identical to those of U . Its last column reads

$$\begin{bmatrix} \int_{W_S \times W_T} (m(s, t_0) - m(s, t)) \lambda(s, t; \zeta) ds dt \\ \int_{W_S \times W_T} (m(s, t_0) - m(s, t)) V(s, t) \lambda(s, t; \zeta) ds dt \\ \int_{W_S \times W_T} (m(s, t_0) - m(s, t))^2 \lambda(s, t; \zeta) ds dt \end{bmatrix}. \quad (14)$$